ELSEVIER

NeuroImage

www.elsevier.com/locate/ynimg
NeuroImage 34 (2007) 204–211

# Connectivity-based parcellation of human cortex using diffusion MRI: Establishing reproducibility, validity and observer independence in BA 44/45 and SMA/pre-SMA

Johannes C. Klein,[a] Timothy E.J. Behrens,[a] Matthew D. Robson,[b] Clare E. Mackay,[b,c] Desmond J. Higham,[d] and Heidi Johansen-Berg[a,*]

[a]*Oxford Centre for Functional Magnetic Resonance Imaging of the Brain, University of Oxford, John Radcliffe Hospital, Oxford OX3 9DU, UK*
[b]*University of Oxford Centre for Clinical Magnetic Resonance Research, John Radcliffe Hospital, Oxford OX3 9DU, UK*
[c]*POWIC, University Department of Psychiatry, The Warneford Hospital, Oxford OX3 7JX, UK*
[d]*Department of Mathematics, University of Strathclyde, Glasgow G1 1HX, UK*

Received 25 February 2006; revised 11 August 2006; accepted 18 August 2006
Available online 3 October 2006

**The identification of specialized, functional regions of the human cortex is a vital precondition for neuroscience and clinical neurosurgery. Functional imaging modalities are used for their delineation in living subjects, but these methods rely on subject cooperation, and many regions of the human brain cannot be activated specifically.**

**Diffusion tractography is a novel tool to identify such areas in the human brain, utilizing underlying white matter pathways to separate regions of differing specialization. We explore the reproducibility, generalizability and validity of diffusion tractography-based localization in four functional areas across subjects, timepoints and scanners, and validate findings against fMRI and post-mortem cytoarchitectonic data. With reproducibility across modalities, clustering methods, scanners, timepoints, and subjects in the order of 80–90%, we conclude that diffusion tractography represents a useful and objective tool for parcellation of the human cortex into functional regions, enabling studies into individual functional anatomy even when there are no specific activation paradigms available.**


## Introduction

The identification of functionally disparate regions of the human cortex in individual subjects is an important aspect of neurosurgery and a prerequisite to many modern methods in neuroscience. To gain insight into functional relationships and networks, techniques such as transcranial magnetic stimulation (TMS) rely on the precise definition of valid targets (Paus et al., 1997). Furthermore, functional regions are taken into account when planning for neurosurgery (Thiel et al., 1998) to minimize post-operative functional deficits and maximize patient benefit in tumor surgery (Proescholdt et al., 2005).

The current gold standard for delineation of specialized regions in the human brain is post-mortem analysis of cyto- or myeloarchitecture (Brodmann, 1909; Economo et al., 1925), which enables parcellation of the human cortex on an objective basis (Schleicher et al., 1999) at microscopic resolution.

For in vivo studies, this kind of data has not been available so far. Consequently, surrogate markers serve to define these regions: for some regions, such as primary sensory and motor cortex, targets can be reliably identified by segmenting anatomical MR images using gross landmarks such as sulci (Geyer et al., 1996, 1999; Yousry et al., 1997), but this approach cannot be reliably used in all regions of cortex: considerable disagreement between anatomical landmarks and functional borders has been observed in other regions (Amunts et al., 1999).

Traditionally, the in vivo identification of functional regions in the human cortex relies upon functional imaging methods such as functional magnetic resonance imaging (fMRI) or positron emission tomography (PET), where a subject performs a task to activate the region under study while being scanned. Such tasks, however, are not available for many areas of interest. Also, functional mapping experiments rely on the subject's ability to understand and perform the task correctly. This task compliance can be impaired in the diseased, in children and in elderly subjects, or where language barriers cannot easily be overcome.

Naturally, areas within a functional network need to interchange information, and underlying white matter projections for these networks have been characterized in post-mortem studies (Flechsig, 1876, 1883).

In recent years, diffusion tensor imaging (DTI) has been introduced as a means to measure cerebral white matter fiber distributions in vivo, bridging the gap between functional imaging methods and anatomical ex vivo approaches. Connectivity between regions of the brain can now be measured in vivo with probabilistic diffusion tractography (Behrens et al., 2003b; Parker et al., 2003; Rushworth et al., 2005). Relationships between preferred con-

* Corresponding author. Fax: +44 1865 222717.
*E-mail address:* heidi@fmrib.ox.ac.uk (H. Johansen-Berg).
**Available online on ScienceDirect (www.sciencedirect.com).**

1053-8119/$ - see front matter © 2006 Elsevier Inc. All rights reserved.
doi:10.1016/j.neuroimage.2006.08.022

nectivity to other regions and regional brain function have been demonstrated. Various different approaches were undertaken to analyze the connection patterns measured, creating parcellations of brain regions solely on the basis of their interconnections with other portions of the brain (Behrens et al., 2003a; Behrens and Johansen-Berg, 2005; Johansen-Berg et al., 2004, 2005). This new enabling technology offers insight into connectional architecture, but there is only sparse validation of its functional implications and reliability.

In an initial approach, a priori target areas were defined comprising regions of the human cortex that different nuclei in the thalamus were expected to connect to (Behrens et al., 2003a; Johansen-Berg et al., 2005). They served as a model driving segmentation, where each voxel in thalamus was assigned to the target region it connected to most strongly. Then, a semi-automated approach using spectral reordering of connectivity matrices followed to parcellate cortical areas without using a priori information about postulated target regions (Johansen-Berg et al., 2004). Connectivity profiles for every voxel in a seed mask were generated, where connection probabilities to every other voxel in the brain are quantified. Then, these connectivity profiles are reordered such that seed voxels with similar connectivity patterns are positioned together in a cross-correlation matrix. A human observer finally selects cut-off points in the connectivity matrix to separate regions with different profiles. An alternative approach, using *k*-means clustering to identify regions of distinct connectivity objectively has also been shown to subdivide lateral premotor (Anwander et al., 2005) and inferior frontal areas (Anwander et al., 2006).

Although these approaches offer substantial promise, there are a number of outstanding questions regarding their reproducibility, generalizability, and validity. Aside from the aforementioned pilot studies, there are no data yet on inter-session and inter-subject reliability of DTI-based brain segmentation. Here, we test an automated approach to parcellation of human cortical regions that does not rely on manual selection of cluster borders, removing observer bias from the analysis process.

We use this approach to differentiate between regions previously shown to be characterized by differing connectivity, namely SMA (Supplementary Motor Area) and pre-SMA (Johansen-Berg et al., 2004), and Brodmann's areas 44 and 45 (Anwander et al., 2006).

SMA is an area that is important in the temporal organization of movements and contains a somatotopic representation of the body, just like the primary motor cortex (Goldberg, 1985; Tanji, 2001), while pre-SMA plays a more abstract role (Picard and Strick, 1996): it is active in the planning and preparation of movement, initiation of movement on cues, acquisition of new motor skills, and higher order aspects of speech, such as self-ordered number generation (Petrides et al., 1993). Brodmann's areas 44 and 45 are part of Broca's area on the left side of the brain, a part of the brain that deals with the understanding and generation of speech. They are particularly active in semantic processing (area 45) and integrating sensory information with motor patterns (area 44) (Gough et al., 2005), and play a key role in the implementation of natural language grammar (Friederici, 2004) and phonological processing.

For SMA vs. pre-SMA, where functional localizer tasks exist, we validate results against findings from functional magnetic resonance imaging (fMRI). For BA44/45, where it is more challenging to identify reliable functional localizers (Amunts et al., 1999; Cabeza and Nyberg, 2000), we validate segmentations against population maps based on cytoarchitectonic data as well as a previously published semi-automated approach with manual division of a spectrally reordered connectivity matrix. Using data acquired in the same subjects on 3 different days, and on two different scanners, we quantify the reproducibility of these approaches.

## Materials and methods

### *Data acquisition*

#### *Pre-SMA vs. SMA*

A detailed description of data acquisition for pre-SMA vs. SMA is available in Johansen-Berg et al. (2004). In brief, nine healthy volunteers (age 24–35, five male) underwent DTI scanning on a 1.5 T Sonata MR scanner (Siemens, Erlangen, Germany) using the standard quadrature head coil supplied with the system. Diffusion was measured in 60 isotropically distributed directions using echo-planar imaging (SE-EPI, TE 97 ms, TR 10.1 s, 72 axial slices, voxel size 2 mm × 2 mm × 2 mm) using a *b*-value of 1000 s mm$^{-2}$. To increase signal to noise ratio (SNR), scanning was repeated three times for averaging, requiring a total scanning time of approximately 45 min. Blood oxygen level-dependent (BOLD) fMRI data were acquired using GE-EPI (20 axial slice, voxel size 2 mm × 2 mm × 5 mm, TE 45 ms, TR 2.5 s). During fMRI, subjects alternated between 30 s blocks of finger tapping, serial subtraction (counting back in threes from a visually presented three-digit number) and rest (ABACACAB, 3.5 repetitions). To ensure compliance, finger tapping was performed using a button box, and subjects were asked to enter the result of their calculation using the same button box at the end of the counting block. The total scanning time for fMRI was approximately 15 min.

#### *Areas 44 vs. 45*

Eight volunteers underwent DTI scanning on a 1.5 T Sonata scanner (4 men, 4 women, age range 21–34 years) on three different days using the protocol mentioned above. Four of the volunteers also received a fourth scan on a 3 T Siemens Trio system (sequence adjusted for TE 106 ms, TR 13.8 s), utilizing the Trio's standard quadrature head coil.

### *Data analysis*

#### *Common space*

While DTI and fMRI analyses were carried out in native acquisition space, result images were stored in MNI152 space in both cases to enable comparison across modalities, scanners and sessions. MNI152 space refers to the space defined by a template generated at the Montréal Neurological Institute, where 152 stereotaxically normalized, T1-weighted scans were averaged to form a standard representation of the human brain. This standard template is distributed with FSL. Correspondence between MNI and acquisition space was determined using two-step affine registration (Jenkinson and Smith, 2001): first, transformation parameters were determined to register the functional image in question to a structural image obtained from the same volunteer. Then, registration parameters were obtained taking the structural image into MNI152 standard space. Both transformation matrices were concatenated to obtain a transform that takes the functional results into standard space.

#### *fMRI analysis*

fMRI data were analyzed using FMRIB's software library (http://www.fmrib.ox.ac.uk/fsl) (Smith et al., 2004). Data were motion corrected (Jenkinson and Smith, 2001), skull-stripped

(Smith, 2002), spatially smoothed with a Gaussian kernel (full width at half maximum 3 mm), intensity-normalized, and then temporally high-pass filtered using a Gaussian-weighted least-squares fit with a filter of $\sigma = 57$ s. Statistical analysis was performed using FILM software with local autocorrelation correction (Woolrich et al., 2001). $Z$ statistic images were computed from original $T$ statistics and a threshold level of $p = 0.01$ was applied. Parameters for affine registration to MNI152 space were determined using individual's structural images.

One subject was excluded from further analysis due to poor fMRI response (fewer than 150 voxels activated during the subtraction task).

*DTI analysis*

Diffusion data were corrected for eddy currents and head motion by affine registration to a reference volume. The three acquisitions collected for each timepoint were averaged to increase SNR. Then, probability distributions of fiber directions were calculated for each brain voxel using FMRIB's Diffusion Toolbox. In brief, probability distributions of fiber orientation are estimated at every voxel. These distributions' widths correspond to the uncertainty associated with the estimated fiber direction. Uncertainty is derived from noise and artifacts in MR imaging, but also from incomplete modeling of the acquired diffusion data, which models one fiber population in every voxel, even though there may be other co-existing fiber populations. Using this knowledge about local probability distributions, probabilistic diffusion tractography can then estimate the pathways that pass through any given seed voxel, as well as the probability that such a pathway will pass through any other voxel in the brain (Behrens et al., 2003a,b).

For pre-SMA vs. SMA, a medial frontal mask was created in MNI152 space. This mask was translated into each subject's native DTI space for tractography. For areas 44 and 45, cytoarchitectonic probability data for both areas from FZ Jülich's SPM Anatomy toolbox (Eickhoff et al., 2005) were thresholded at 20% minimum probability and transformed into MNI152 space using affine registration (Jenkinson and Smith, 2001). The two datasets were summed and binarized, and a sagittal slice was selected as seed mask.

For both studies, probabilistic tractography was run from every voxel in the respective mask to assess connectivity with every brain voxel. All tracking was performed in original DTI space but data were stored in seed space, the MNI152 space referred to earlier. For reasons of data storage, brain voxel space was sub-sampled to lower resolution (5 mm × 5 mm × 5 mm). Connectivity was expressed as the number of particles from the seed voxel traveling through the low-resolution brain voxel in question. Information about connectivity was stored in an $M$-by-$N$ matrix, where $M$ denotes the number of voxels in the seed mask and $N$ the number of voxels in low-resolution brain space. Cross-correlation (CC) between the connectivity patterns of all $M$ voxels in the seed mask were calculated and stored in an $M$-by-$M$ CC matrix (cf., Fig. 1, leftmost).

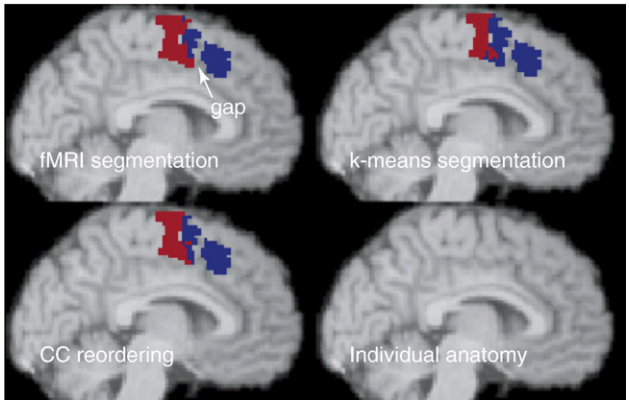


Fig. 2. Overview of the strategies used for pre-SMA vs. SMA segmentation using fMRI, *k*-means clustering of DTI data and spectral reordering of the CC matrix. Note the gap in fMRI results.

*Classification by spectral reordering*

This matrix was then reordered using a spectral-reordering algorithm, minimizing the sum of the element value (CC value) multiplied by the square of its distance to the matrix diagonal. The idea is to put nodes close together if they are strongly connected. It is not feasible to exhaustively search over all reorderings, so the Fiedler approach exactly solves a related problem that has continuous variables. For an in-depth discussion of this approach, cf. Higham et al. (2006).

Potential clusters in the data will show up in the reordered matrix and can be manually identified. A cut-off point was defined by eye where there was a break in the connectivity pattern, dividing the matrix into two subsets. As knowledge about the location of the $M$ seed voxels is retained throughout processing, the two subsets can now be defined in volume space. The center of mass is calculated for each, and the one with the more anterior coordinate defines which of the two is pre-SMA or area 45, respectively.

*Automated classification using k-means segmentation*

The $M$-by-$M$ CC matrix was fed into *k*-means segmentation for automated clustering. The implementation uses the algorithm published in Hartigan (1975). 200 iterations with a predetermined

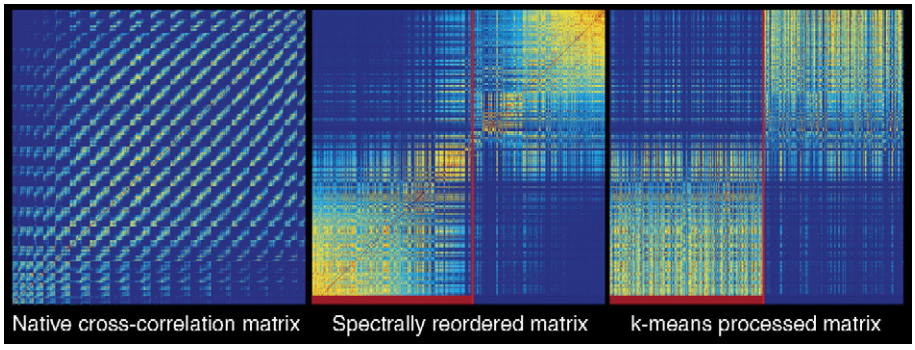


Fig. 1. The CC matrix in its native state, spectrally reordered, and *k*-means classified. The bright red line indicates points of cluster separation.

number of two clusters were performed, resulting in two subsets of the M seed voxels. *k*-means clustering starts by randomly assigning the columns of the matrix, equivalent to each voxel's CC characteristics, to one of the two clusters. Then, the iterative process strives to minimize the variability within the clusters, while maximizing the variability between them. This is achieved by (a) computing the centroid of each cluster and (b) re-assigning the elements to the clusters such that their squared difference from the centroid is minimal. These steps are alternated until the preset number of iterations is reached. This approach minimizes the mean squared difference of each cluster's elements from its centroid, while maximizing the squared difference between cluster centroids.

In the case of pre-SMA vs. SMA, only voxels that had been significantly activated in the fMRI study were selected for further processing, but clustering was performed beforehand on the full seed mask.

Fig. 1 depicts the CC matrix in its native state, where its elements' positions are solely determined by voxel location in the seed mask. Further processing results in the spectrally reordered and the *k*-means classified versions, where a red bar indicates cut-off between clusters (manually selected in the former, automatically selected in the latter case).

### *Validation*

#### *pre-SMA vs. SMA*

DTI results of spectral-reordering and *k*-means clustering were validated against fMRI results. Also, agreement between classification through spectral-reordering and *k*-means segmentation was assessed.

Agreement between methods was quantified as the conditional probability that a voxel classified as belonging to a particular region in segmentation $A$ would receive the same classification using segmentation method $B$ as in $P_A(B) = \frac{|A \cap B|}{|A|}$.

For differentiation between pre-SMA and SMA, fMRI results served as the standard against which DTI was being evaluated. Thus, fMRI results correspond to segmentation $A$ in the notation introduced above, resulting in the probability of a voxel being

Table 1
Results of internal and external validation of connectivity-based parcellation of area 44 vs. 45 and pre-SMA vs. SMA

| Internal validation | | | | | | |
|---|---|---|---|---|---|---|
| | Area 44 | | Area 45 | | Overall | |
| | Mean (%) | SD | Mean (%) | SD | Mean (%) | SD |
| *Areas 44 and 45: Areal agreement between timepoints* | | | | | | |
| *k*-means clustering | 88.8 | 0.1302 | 88.2 | 0.1421 | 88.5 | 0.1337 |
| Spectral reordering | 90.5 | 0.0967 | 89.5 | 0.0927 | 90.0 | 0.0925 |
| Average across methods | 89.7 | 0.1147 | 88.8 | 0.1200 | 89.3 | 0.1150 |
| *Areal agreement between 1.5 T and 3 T scans* | | | | | | |
| *k*-means clustering | 88.9 | 0.1371 | 88.9 | 0.1495 | 88.9 | 0.1374 |
| Spectral reordering | 86.6 | 0.0749 | 85.6 | 0.0391 | 86.1 | 0.0580 |
| Average across methods | 87.7 | 0.1105 | 87.3 | 0.1093 | 87.5 | 0.1055 |
| *Areal agreement between clustering methods* | | | | | | |
| *k*-means clustering vs. spectral reordering | 93.3 | 0.0509 | 93.5 | 0.0637 | 93.4 | 0.0576 |
| | pre-SMA | | SMA | | Overall | |
| | Mean (%) | SD | Mean (%) | SD | Mean (%) | SD |
| *pre-SMA and SMA: Areal agreement between clustering methods* | | | | | | |
| *k*-means clustering vs. spectral reordering | 90.9 | 0.0684 | 93.6 | 0.0625 | 92.2 | 0.0649 |

| External validation | | | | |
|---|---|---|---|---|
| | Area 44 | | Area 45 | |
| | Mean (%) | SD | Mean (%) | SD |
| *Area 44 and 45: Recovery of cytoarchitectonic probabilities* | | | | |
| *k*-means clustering: recovered cytoarchitectonic probability | 38.8 | 0.0194 | 47.1 | 0.0532 |
| –As percentage of ideal segmentation | 95 | | 90 | |
| Spectral reordering: recovered cytoarchitectonic probability | 38.9 | 0.0181 | 48.9 | 0.0395 |
| –As percentage of ideal segmentation | 95 | | 93 | |
| Average across methods | 38.9 | 0.0188 | 48.0 | 0.0469 |
| –As percentage of ideal segmentation | 95 | | 92 | |
| For reference, an ideal segmentation would recover | 40.9 | | 52.4 | |
| | pre-SMA | | SMA | |
| *pre-SMA and SMA: Classification agreement between fMRI and DTI results* | | | | |
| Concordant classification with *k*-means clustering and fMRI | 82 | 0.167 | 79 | 0.143 |
| Concordant classification with spectral reordering and fMRI | 74 | 0.184 | 87 | 0.133 |

classified as (pre-) SMA by DTI given its known designation from fMRI.

*Area 44 vs. area 45*

For establishing reproducibility in the segmentation of area 44 vs. 45, there is no such standard. Thus, computation of conditional probability in each pair of acquisitions in a given subject was performed twice, crossing over the segmentations between runs.

For each pair $A$ and $B$ of acquisitions, $P_A(B)$and $P_B(A)$were then averaged to give the overall, bilateral conditional probability of concordant classification.

Equally, bilateral conditional probabilities were calculated to assess agreement between clustering approaches in all scans of both studies.

## Results

*Validation of medial frontal segmentation*

Fig. 2 displays a sagittal slice through a typical result, comparing fMRI and both DTI approaches.

Internal validation, expressed as bilateral conditional probability of concordant classification, demonstrated an agreement between both DTI-based clustering approaches of 92%. External validation of DTI against fMRI results, expressed as likelihood of correct classification with DTI-based approaches given the fMRI result, established an average likelihood of concordant classification of 74–87% (cf., Table 1 for detailed results).

*Validation of area 44 vs. 45 segmentation*

In Fig. 3, data from a single subject over all timepoints studied are summarized, depicting a well-reproduced cut-off line across the different acquisitions.

Internal validation showed agreement between clustering methods of 93.4%. Average reproducibility across timepoints was 89.3%, while reproducibility between the two scanners used was 87.5% (cf., Table 1, also see Supplementary Material for details).

External validation was performed against cytoarchitectonic data. Due to the probabilistic nature of the cytoarchitectonic maps, the maximum recoverable probability is 40.9% for area 44 and 52.4% for area 45. Results of clustering are expressed as a percentage of these maximum achievable values.

Average recovery of cytoarchitectonic probability was 92 and 95% of the maximum possible value for area 44 and 45 (cf., Table 1 for detailed results).

Summed-up images of recovered cytoarchitecture are displayed in Fig. 4, showing good agreement between the expected distri-

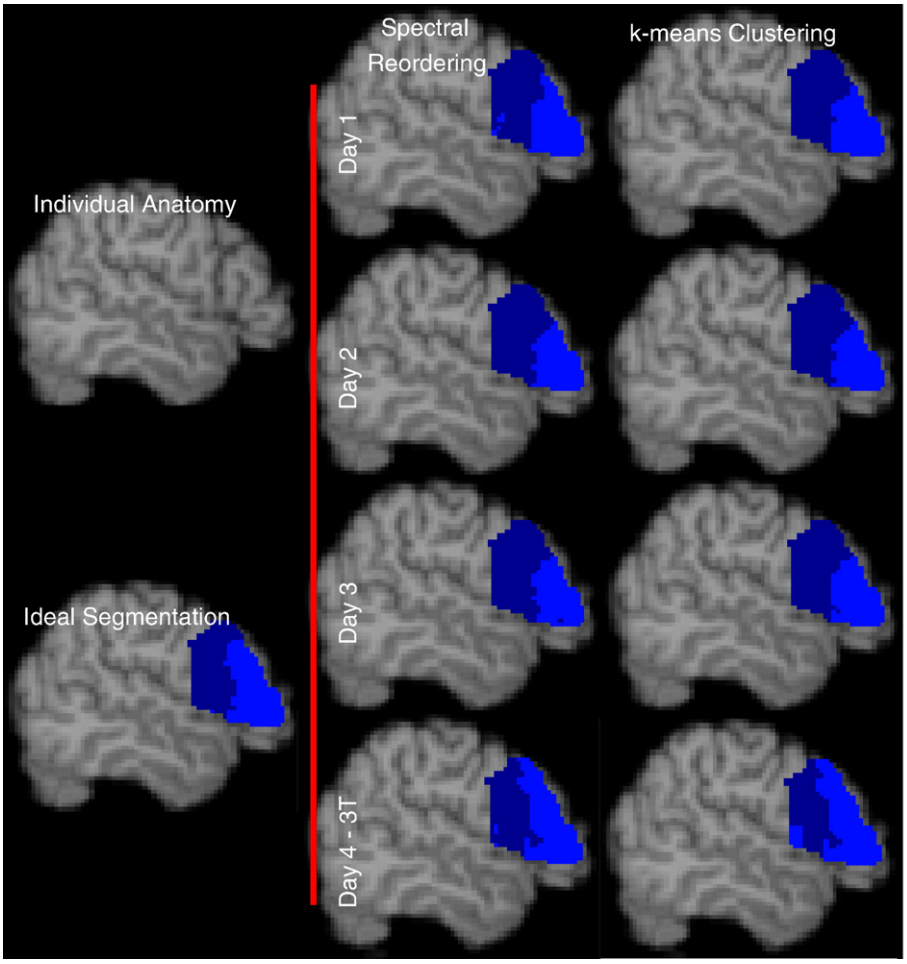


Fig. 3. Reproducibility is established in a subject across dates and scanners. For comparison, we depict individual anatomy and an ideal segmentation based on cytoarchitectonic probabilities.

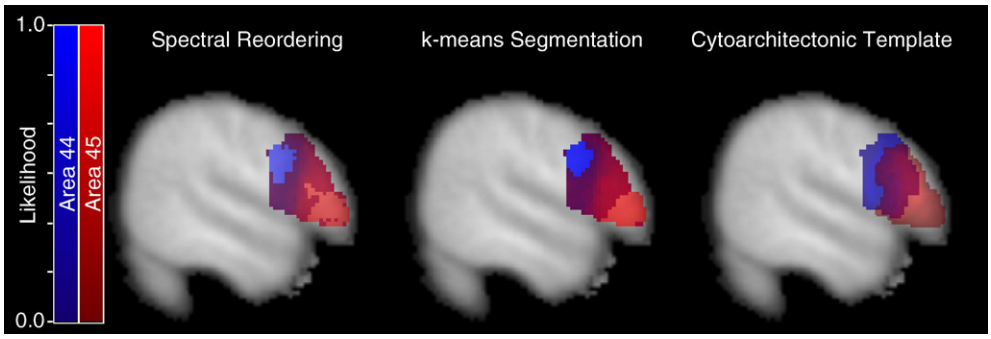


Fig. 4. Likelihood of voxel classification as area 44 (blue) and area 45 (red) in our study collective using spectral-reordering and *k*-means segmentation of the CC matrix is compared to established cytoarchitectonic data.

bution as predicted via cytoarchitectonic maps and the actual distribution of areas measured in our study collective.

Data on individual subject level are provided online as Supplementary Material.

## Discussion

Probabilistic diffusion tractography is a novel, non-invasive tool in the analysis of structural and functional brain anatomy, and parcellation of the human brain into functional areas is one of its newest applications (Anwander et al., 2006; Johansen-Berg et al., 2004). However, extending the use of such parcellations requires validation of this approach by demonstrating its reproducibility over time as well as across subjects and scanners. We have now demonstrated feasibility, accuracy, repeatability and subject and scanner independence of an automated parcellation of four different areas in the human cortex based on probabilistic diffusion tractography, enabling subject-specific segmentation of functional regions even where activation tasks may offer ambiguous results (Cabeza and Nyberg, 2000). Moreover, using *k*-means clustering, manual interaction is minimized and classification is more objective than in the previously published approach (Johansen-Berg et al., 2004).

Connectivity-based parcellation of grey matter has been previously demonstrated in medial (Johansen-Berg et al., 2004) and inferior (Anwander et al., 2006) frontal cortex and the data presented here suggests that parcellation in these regions is reproducible and reliable. Generalizability of the approach to other brain regions, however, has yet to be fully tested. For both regions tested so far, we have strong a priori expectations of the number of anatomical subregions that should be present, and therefore, certain limitations of the clustering approaches employed (such as having to decide on the number of clusters to separate for *k*-means clustering) are not serious. As we extend the approach to other brain regions, however, it will become increasingly important to explore techniques for automatic determination of the optimal number of clusters for separation (Girolami, 2002; Sanguinetti et al., 2005). Another feature of the cortical areas subdivided so far is that the different regions have quite distinct connectivity patterns and so cross-correlation in connectivity between regions is low and separation of clusters is clear. In other brain areas, such as the visual cortices, adjacent regions may have more similar connection patterns and so divisions become less clear cut. Exploration of methods such as fuzzy clustering could prove useful for parcellation in such regions.

Separation of pre-SMA and SMA was highly consistent with findings from fMRI. It should be noted that the separation line predicted by DTI analysis, as depicted in Fig. 2, does not coincide with the gap in the fMRI-generated mask or a sulcal line. The former could suggest an artificial separation that benefits from the fact that any coincidental separation line across the gap would seem to separate pre-SMA from SMA, while the latter might be due to local phenomena of fiber dispersion at the fundus of a sulcus. Instead, the separation agrees with the functionally defined separation in the same figure.

The agreement of the different DTI techniques with fMRI results is about 80%. The spectral-reordering (Johansen-Berg et al., 2004) and *k*-means (Anwander et al., 2006) approaches proposed previously gave similar results in the examples shown here. The *k*-means approach, however, has the advantage that the boundary between clusters is identified objectively and does not have to be determined by eye.

Separation of areas 44 and 45 of Brodmann was consistent with their known distribution from cytoarchitectonic studies, as Fig. 4 and recovered probability around 95% illustrate. Remarkably, the blending occurring between the two areas is very similar to the distribution of probability that cytoarchitectonic analyses established (Fig. 4). Those offer the most accurate method of separation available to date, but are naturally available only for post-mortem analysis.

If the approaches described here successfully generalize to other regions of cortex, then parcellation based on anatomical connectivity could help bridge the gap that has so far existed between ex vivo anatomical and in vivo functional methods. By allowing for identification of likely microstructural borders in vivo, these approaches should enable further investigation of structure–function relationships in the living human brain.

Some factors impact data quality in DTI scanning more than in other EPI-based imaging approaches. The diffusion-weighted sequence used suffers from the same B0 distortion problems that BOLD imaging is notorious for, but additionally, induction of eddy currents in metal parts of the scanner during each diffusion gradient adds further image distortion. As explained above, we can correct for that using affine registration, but inevitably, these effects cannot be removed completely. Furthermore, contrast-to-noise is considerably lower, owing to the fact that diffusion gradients need to be applied for a certain period of time, which gives the excited spins more time to decay. Long TR also means that fewer excitations can be performed in a given amount of time.

While the initial signal at a field strength of 3 T is higher, T2* contrast decays more rapidly than at 1.5 T, and the greater distortions in B0 give rise to more pronounced artifacts as these effects scale linearly with field strength. Our analysis shows that the negative aspects of the aforementioned effects does not significantly impact DTI in the areas under study, with reprodu-

cibility of 87.5% between 1.5 T and 3 T acquisitions, which is virtually identical to the overall reproducibility of 89.3%. Advances in scanner technology and sequence design (Andersson et al., 2003; Bodurka et al., 2004; Gizewski et al., 2005) are expected to resolve some of the technical issues presented and make 3 T more attractive as an imaging platform. Parallel imaging techniques making use of array coils aim to significantly reduce the amount of distortion, and also the scanning time. The latter is particularly desirable in a clinical setting.

Given the current resolution available for DTI data, all major fiber pathways can be traced. Still, improvements in DTI resolution are desirable, as they will extend the scope of fiber populations that can be explored.

Further analysis will need to assess if these methods are also applicable to the diseased brain, which would offer an objective way to identify specific target structures prior to neurosurgery, and also to help avoid functional deficits in invasive procedures, even when communication with and cooperation of a patient are impaired.

## Acknowledgments

We are grateful for financial support from the UK BBSRC (J.K.), UK MRC (H.J.B., T.B.) and Wellcome Trust (H.J.B.).

## Appendix A. Supplementary data

Supplementary data associated with this article can be found, in the online version, at doi:10.1016/j.neuroimage.2006.08.022.

## References

Amunts, K., Schleicher, A., Burgel, U., Mohlberg, H., Uylings, H.B.M., Zilles, K., 1999. Broca's region revisited: cytoarchitecture and intersubject variability. Journal of Comparative Neurology 412, 319–341.

Andersson, J.L.R., Skare, S., Ashburner, J., 2003. How to correct susceptibility distortions in spin-echo echo-planar images: application to diffusion tensor imaging. NeuroImage 20, 870–888.

Anwander, A., Schubotz, R.I., Tittgemeyer, M., Brass, M., Knösche, T.R., 2005. DTI-Tractography Based Parcellation of Human Precentral Gyrus. OHBM 2005, Toronto, Canada.

Anwander, A., Tittgemeyer, M., von Cramon, D.Y., Friederici, A.D., Knosche, T.R., 2006. Connectivity-based parcellation of Broca's area. Cereb.Cortex.

Behrens, T.E.J., Johansen-Berg, H., 2005. Relating connectional architecture to grey matter function using diffusion imaging. Philosophical Transactions of the Royal Society B-Biological Sciences 360, 903–911.

Behrens, T.E.J., Johansen-Berg, H., Woolrich, M.W., Smith, S.M., Wheeler-Kingshott, C.A.M., Boulby, P.A., Barker, G.J., Sillery, E.L., Sheehan, K., Ciccarelli, O., Thompson, A.J., Brady, J.M., Matthews, P.M., 2003a. Non-invasive mapping of connections between human thalamus and cortex using diffusion imaging. Nature Neuroscience 6, 750–757.

Behrens, T.E.J., Woolrich, M.W., Jenkinson, M., Johansen-Berg, H., Nunes, R.G., Clare, S., Matthews, P.M., Brady, J.M., Smith, S.M., 2003b. Characterization and propagation of uncertainty in diffusion-weighted MR imaging. Magnetic Resonance in Medicine 50, 1077–1088.

Bodurka, J., Ledden, P.J., van Gelderen, P., Chu, R.X., de Zwart, J.A., Morris, D., Duyn, J.H., 2004. Scalable multichannel MRI data acquisition system. Magnetic Resonance in Medicine 51, 165–171.

Brodmann, K., 1909. Vergleichende Lokalisationslehre der Grosshirnrinde in ihren Prinzipien dargestellt auf Grund des Zellenbaues. J. A. Barth, Leipzig.

Cabeza, R., Nyberg, L., 2000. Imaging cognition II: an empirical review of 275 PET and fMRI studies. Journal of Cognitive Neuroscience 12, 1–47.

Economo, C., Koskinas, G.N., Wagner-Jauregg, J.v., 1925. Die Cytoarchitektonik der Hirnrinde des erwachsenen Menschen. J. Springer, Wien, Berlin.

Eickhoff, S.B., Stephan, K.E., Mohlberg, H., Grefkes, C., Fink, G.R., Amunts, K., Zilles, K., 2005. A new SPM toolbox for combining probabilistic cytoarchitectonic maps and functional imaging data. NeuroImage 25, 1325–1335.

Flechsig, P.E., 1876. Die Leitungsbahnen im Gehirn und Rückenmark des Menschen, auf Grund entwickelungsgeschichtlicher Untersuchungen. Engelmann, Leipzig.

Flechsig, P.E., 1883. Plan des menschlichen Gehirns: auf Grund eigener Untersuchungen entworfen. Veit, Leipzig.

Friederici, A.D., 2004. Processing local transitions versus long-distance syntactic hierarchies. Trends Cogn. Sci. 8, 245–247.

Geyer, S., Ledberg, A., Schleicher, A., Kinomura, S., Schormann, T., Burgel, U., Klingberg, T., Larsson, J., Zilles, K., Roland, P.E., 1996. Two different areas within the primary motor cortex of man. Nature 382, 805–807.

Geyer, S., Schleicher, A., Zilles, K., 1999. Areas 3a, 3b, and 1 of human primary somatosensory cortex 1. microstructural organization and interindividual variability. NeuroImage 10, 63–83.

Girolami, M., 2002. Mercer kernel-based clustering in feature space. Ieee Transactions on Neural Networks 13, 780–784.

Gizewski, E.R., Maderwald, S., Wanke, I., Goehde, S., Forsting, M., Ladd, M.E., 2005. Comparison of volume, four- and eight-channel head coils using standard and parallel imaging. European Radiology 15, 1555–1562.

Goldberg, G., 1985. Supplementary motor area structure and function: review and hypotheses. Behav. Brain Sci. Behavioral and brain sciences (Behav. brain sci.) 567–615.

Gough, P.M., Nobre, A.C., Devlin, J.T., 2005. Dissociating linguistic processes in the left inferior frontal cortex with transcranial magnetic stimulation. J. Neurosci. 25, 8010–8016.

Hartigan, J.A., 1975. Clustering algorithms. Wiley, New York; London (etc.).

Higham, D.J., Kalna, G., Kbble, M., 2006. Spectral clustering and its use in bioinformatics. Journal of Computational and Applied Mathematics.

Jenkinson, M., Smith, S., 2001. A global optimisation method for robust affine registration of brain images. Medical Image Analysis 5, 143–156.

Johansen-Berg, H., Behrens, T.E., Robson, M.D., Drobnjak, I., Rushworth, M.F., Brady, J.M., Smith, S.M., Higham, D.J., Matthews, P.M., 2004. Changes in connectivity profiles define functionally distinct regions in human medial frontal cortex. Proc. Natl. Acad. Sci. U. S. A. 101, 13335–13340.

Johansen-Berg, H., Behrens, T.E.J., Sillery, E., Ciccarelli, O., Thompson, A.J., Smith, S.M., Matthews, P.M., 2005. Functional–anatomical validation and individual variation of diffusion tractography-based segmentation of the human thalamus. Cerebral Cortex 15, 31–39.

Parker, G.J.M., Haroon, H.A., Wheeler-Kingshott, C.A.M., 2003. A framework for a streamline-based probabilistic index of connectivity (PICo) using a structural interpretation of MRI diffusion measurements. Journal of Magnetic Resonance Imaging 18, 242–254.

Paus, T., Jech, R., Thompson, C.J., Comeau, R., Peters, T., Evans, A.C., 1997. Transcranial magnetic stimulation during positron emission tomography: a new method for studying connectivity of the human cerebral cortex. Journal of Neuroscience 17, 3178–3184.

Petrides, M., Alivisatos, B., Meyer, E., Evans, A.C., 1993. Functional activation of the human frontal-cortex during the performance of verbal working memory tasks. Proceedings of the National Academy of Sciences of the United States of America 90, 878–882.

Picard, N., Strick, P.L., 1996. Motor areas of the medial wall: a review of their location and functional activation. Cerebral Cortex 6, 342–353.

Proescholdt, M.A., Macher, C., Woertgen, C., Brawanski, A., 2005. Level of evidence in the literature concerning brain tumor resection. Clinical Neurology and Neurosurgery 107, 95–98.

Rushworth, M.F., Behrens, T.E., Johansen-Berg, H., 2005. Connection patterns distinguish 3 regions of human parietal cortex. Cerebral Cortex 16, 1418–1430.

Sanguinetti, G., Laidler, J., Lawrence, N.D., 2005. Automatic determination of the number of clusters using spectral algorithms. Proceedings of the IEEE MLSP, pp. 55–60.

Schleicher, A., Amunts, K., Geyer, S., Morosan, P., Zilles, K., 1999. Observer-independent method for microstructural parcellation of cerebral cortex: a quantitative approach to cytoarchitectonics. NeuroImage 9, 165–177.

Smith, S.M., 2002. Fast robust automated brain extraction. Human Brain Mapping 17, 143–155.

Smith, S.M., Jenkinson, M., Woolrich, M.W., Beckmann, C.F., Behrens, T. E.J., Johansen-Berg, H., Bannister, P.R., De Luca, M., Drobnjak, I., Flitney, D.E., Niazy, R.K., Saunders, J., Vickers, J., Zhang, Y.Y., De Stefano, N., Brady, J.M., Matthews, P.M., 2004. Advances in functional and structural MR image analysis and implementation as FSL. NeuroImage 23, S208–S219.

Tanji, J., 2001. Sequential organization of multiple movements: involvement of cortical motor areas. Annual Review of Neuroscience 24, 631–651.

Thiel, A., Herholz, K., von Stockhausen, H.M., Leyen-Pilgram, K., Pietrzyk, U., Kessler, J., Wienhard, K., Klug, N., Heiss, W.D., 1998. Localization of language-related cortex with O-15-labeled water PET in patients with gliomas. NeuroImage 7, 284–295.

Woolrich, M.W., Ripley, B.D., Brady, M., Smith, S.M., 2001. Temporal autocorrelation in univariate linear modeling of fMRI data. NeuroImage 14, 1370–1386.

Yousry, T.A., Schmid, U.D., Alkadhi, H., Schmidt, D., Peraud, A., Buettner, A., Winkler, P., 1997. Localization of the motor hand area to a knob on the precentral gyrus—A new landmark. Brain 120, 141–157.